Available online at www.sciencedirect.com
ScienceDirect
Applied Catalysis A: General 326 (2007) 227–235
APPLIED CATALYSIS A: GENERAL
www.elsevier.com/locate/apcata

Carbon-supported low-loading rhodium sulfide electrocatalysts for oxygen depolarized cathode applications

Andrea F. Gullá [a,*], Lajos Gancs [b], Robert J. Allen [a], Sanjeev Mukerjee [b]

[a] *E-TEK Division of PEMEAS Fuel Cell Technologies, 39 Veronica Avenue Somerset, NJ 08873, USA*
[b] *Northeastern University, Department of Chemistry and Chemical Biology, Boston, MA 02115, USA*

Received 18 January 2007; received in revised form 9 April 2007; accepted 12 April 2007
Available online 20 April 2007

Abstract

Noble metal chalcogens are the preferred choice of electrocatalyst materials over pure metals and metal alloys in many industrial processes involving operation in highly corrosive environment. The depolarised electrolysis of hydrochloric acid represents one of such processes; in this case, rhodium sulfide is incorporated into gas diffusion electrode structure for use as oxygen-consuming cathode. An increased dispersion of the rhodium/sulfur compound is an evident goal to obtain highly active catalyst systems while maintaining similar activity. In studying the effect of Rh_xS_y loading on carbon on oxygen reduction reaction activity, it is paramount to understand and optimize the structure sensitivity of the reaction. Doing so will not only aid in determining the optimal metal loading but more importantly will control the commercial viability of the electrocatalyst. In the present work, the Rh_xS_y loading on Vulcan XC72-R was studied in terms of morphological characteristics and ORR activity. Physicochemical characterization suggests that the preparation methodology of such chalcogens plays a fundamental role in terms of chemical structure. ORR kinetics was addressed using a series of rotating disk electrode experiments in 1 M HCl electrolyte, in which the optimal Rh_xS_y loading was found to be at 15 wt.%, a value two times lower with respect to the commercially available 30 wt.% material. Any higher dispersion results in no significant increase in the overall electrocatalytic performance. Based on the increased Rh utilization and enhanced activity found for the low-loading Rh_xS_y/C samples, we report a significant development in terms of materials and material employment for the oxygen depolarized electrolysis of HCl.

Keywords: Hydrochloric acid electrolysis; Oxygen-depolarized cathode; Oxygen reduction reaction; Rhodium sulfide

1. Introduction

The electrolysis of aqueous HCl solutions is a widely used industrial method for the recovery of high-value chlorine gas [1]. Aqueous hydrochloric acid is an abundant chemical by-product, especially in chemical plants making use of chlorine as a reactant. In this case, the chlorine evolved in the anodic compartment of the electrolyzer can be recycled as feedstock to the chemical plant. Electrolysis has only recently become remarkably efficient [1–4] when the standard hydrogen-evolving cathode was replaced by an oxygen-consuming gas diffusion electrode (GDE). The efficiency gain is mainly due to the associated decrease in energy consumption needed to operate the system (corresponding to a lowering of over-potential by as much as 1 V). The ability of the gas diffusion electrode to operate successfully in this environment is crucially dependent on the nature and performance of the catalyst as well as on the structure of the gas diffusion electrode. In conventional hydrochloric acid electrolysis technology, aqueous hydrochloric acid, located at in the anodic compartment of a graphite cell, is electrolysed and separated by the cathodic compartment by a porous diaphragm or a membrane [5–7,1]. The overall cell reaction pathway can be written as:

$$2HCl + \text{electric energy} \Rightarrow Cl_2 + H_2$$

In such configuration, the typical energy input is 1500 kWh/tonne of Cl_2 [8]. In an oxygen depolarized cathode (ODC), oxygen is reduced to hydrogen peroxide or water [4], and the respective anode and cathode reactions are written as follows:

$$2HCl + \text{electric energy} \Rightarrow Cl_2 + 2H^+ + 2e^-$$

$$\tfrac{1}{2}O_2 + 2H^+ + 2e^- + \text{electric energy} \Rightarrow H_2O$$

In this case, when a voltage is applied between the electrodes, protons migrate from the anodic compartment

* Corresponding author. Tel.: +1 617 373 8914; fax: +1 617 373 8949.
E-mail address: a.gulla@etek-inc.com (A.F. Gullá).

0926-860X/$ – see front matter © 2007 Elsevier B.V. All rights reserved.
doi:10.1016/j.apcata.2007.04.013

through a proton exchange membrane and reach the cathodic compartment where oxygen is reduced on a GDE whilst the only by-product of the process is water [8]. According to the above half reactions (anodic and cathodic), the overall cell reaction for the new process changes to:

$$2HCl + \tfrac{1}{2}O_2 + \text{electric energy} \Rightarrow Cl_2 + H_2O$$

As mentioned previously, by utilizing an ODC based process, the cell potential can theoretically be lowered by as much as 1 V entailing energy savings of *ca.* 700 kWh/tonne of Cl_2. The system still utilizes a proton exchange membrane which serves two purposes; it acts primarily as a separator and also as a proton conducting media between the anode and cathode compartments of the cell, similar to the membrane electrode assemblies (MEA) adopted in proton exchange membrane (PEM) fuel cells. The successful operation of a GDE in such highly corrosive and poisoning environment is solely dependent on the stability and activity toward oxygen reduction reaction (ORR) of the electrocatalyst material utilized.

Platinum is generally recognized as the most effective catalyst for the electroreduction of oxygen, especially in the context of low to medium temperature acid environment for fuel cells and electrolyzers. However, in the particular case of aqueous hydrochloric acid electrolysis, the use of platinum-based catalyst as cathode poses some serious drawbacks mainly related to its stability, thus also hindering its catalytic activity. Although the hydrochloric acid solution is not in direct contact with the cathode, its crossover through the polymer electrolyte membrane must be considered. Even at low concentrations, dissolved chloride ions can readily deteriorate the performance of the platinum-based oxygen depolarized cathodes. The dissolution rate of the platinum-group elements (including rhodium) can be substantial [9], mainly resulting from chloride adsorption-induced corrosion but also associated to the inherent solubility of surface hydroxides [10] in strongly acidic solutions (pH < 2). Simultaneously, the strong specific adsorption of chloride ions on these transition metals [11] poses severe kinetic limitations in the ORR while enhancing the production of hydrogen peroxide [9]. In addition to chloride poisoning, platinum can also be deactivated [10] by the inevitable presence of various dissolved organic contaminants in the electrolyte.

From a practical stand point, when using platinum-based GDEs, it is necessary to undertake carefully planned procedures during the periodic system ''shut-down'' cycles. In those situations, any sudden shift in the cathodic potential in the highly corrosive environment, can lead to the dissolution of a significant amount of noble metal and the subsequent deactivation of the remaining portion. While tailored procedures to overcome such catastrophic events during shut-down are planned and generally used in various industrial settings, no contingency exists in the case of uncontrolled events such as those described primarily because resulting from unpredictable and sudden power shortage in the electrical network grid.

Because of the major corrosion issues when employing platinum-group metals or alloys as ODC electrocatalysts, considerable research efforts have been made in the attempt to discover more stable materials. The vast majority of proposed alternatives to platinum are based on non-noble transition metal compounds. Cote et al. [12] have proposed pyrolyzed metal porphyrins based on Fe and Cr, however stability and durability still needs to be addressed for such systems. Other alternatives have been based on the utilization of transition metal carbides with the most popular systems based on tungsten carbides [13–15]. The tungsten carbide materials, nevertheless, suffer from the same durability problems as encountered with the metal porphyrins. Perhaps the most promising system, first reported by Alonso-Vante et al. [16,17] is the family of semiconducting transition metal-based chalcogen clusters. Despite their early promises to be efficient oxygen reduction electrocatalysts in various applications where the platinum-group metals reign was unchallenged, several essential issues concerning their preparation, chemical structure and the electrocatalytic mechanism need yet to be addressed. Generally speaking, one of the major downsides of such family of compounds lies in the fact that their synthesis is quite challenging and difficult to control. In addition, several research groups have presented conflicting opinions regarding the catalytic centres of these complexes [18] and as a result, a vast variety of materials have been examined [4,18–23]. In the past years, some of these problems have been partially addressed with the development of rhodium-based catalyst [2], which despite their lower activity for oxygen reduction relative to Pt, have exhibited significantly higher depolarisation. This behaviour is especially relevant in the context of the presence of chloride ions and other organics [10,19] and enables more acceptable results in terms of operating voltage upon incorporation in a conventional GDE. Even more resistant materials, various kind of rhodium sulfides, have been developed [3,4], which, in contrary to a simple rhodium based catalyst, do not require any conditioning step to completely survive in the highly corrosive operational environment. Although these catalysts show very good performance, both in terms of activity and chemical resistance, their price and availability is a difficult issue to overcome in terms of large commercial applications. Rhodium is one of the most expensive noble metals with a price exceeding that of osmium and being several orders of magnitude higher compared to the price of ruthenium and iridium. Although depolarized aqueous hydrochloric acid electrolysis represents a technology with a high market demand, the price of the state-of-the-art electrocatalysts may be too high to lead to commercialization.

It is the primary object of this work to investigate the effect of Rh_xS_y loading (on carbon) on the ORR when utilised as oxygen depolarized cathodes in the reaction of the electrolysis of aqueous HCl. Of scientific relevance, is the fact that loading, in this case, affects the nature of the chalcogen surface and statistics of active reaction centers. For this investigation a series of Rh_xS_y/C electrocatalysts were synthesized at various loadings (0, 10, 15, 30, and 100 wt.% in respect to carbon), and their bulk and surface physicochemical properties were studied by powder X-ray diffraction, SEM imaging and cyclic voltammetry. A dual role of the carbon support material in the preparation procedure has been discovered: while its porosity and intrinsic surface area determines the dispersion of

chalcogen nanoparticles, its relative amount in respect to the rhodium and sulfur is found to influence the crystal structure as well as the resulting crystal phases of Rh_xS_y prepared. The ORR activity of the supported Rh_xS_y samples were addressed by using rotating disk electrode experiments [22] in oxygen-saturated 1 M HCl solution relevant to conditions in HCl electrolysis cells and benchmarked to those of pure platinum and rhodium nanoparticles. To support the significant improvement observed with the RDE test, single electrolysis cell experiments were also carried out. The results of this study confirmed our cell tests wherein the currently applied 30 wt.% rhodium sulfide loading on the carbon support could effectively be cut in third while maintaining both the same ORR performance. Apart from the more direct and obvious industrial implications targeted to cutting the actual cost of the gas diffusion electrodes, this result also contributes to a better understanding on the ORR performance of the rhodium sulfide system as a function of their physical and chemical structural properties. Our ultimate goal is also to define a more active and stable supported Rh_xS_y thus improving the overall cost efficiency from a system operation standpoint.

2. Experimental

2.1. Electrocatalyst samples and preparation

All the supported Rh_xS_y catalysts as well 30 wt.% supported Pt reference catalyst are the courtesy of *E-TEK* Division of PEMEAS Fuel Cell Technologies, Inc. and prepared accordingly to the procedure described elsewhere [2–4]. To measure the ORR activity of the samples under HCl electrolysis, the powdered samples were incorporated into gas diffusion electrodes (GDE) [24], which were also provided by *E-TEK*. The electrode loading ranged between 0.5 and 1.0 mg/cm^2. All electrodes were coated with 0.5 mg/cm^2 of perfluorocarbon ionomer solution (NAFION®).

2.2. Physical characterization

Morphological characterization of the powdered Rh_xS_y/C samples was carried out on a SEM/EDAX instrument (Hitachi S-4800 Field Emission SEM attached to Genesis 136-10 EDAX EDS unit). The SEM images were taken at different domains of the catalyst surfaces. The crystallographic characterization of the samples was carried out using a Rigaku D/Max-2200V X-ray powder diffractometer (USA) utilizing a 2.0 kW Cu target X-ray tube (Cu $K_{\alpha 1}$ radiation: $\lambda = 1.5405$ Å), a vertical wide-angle goniometer and a high-efficiency scintillation counter providing linearity up to 250 kcps. The spectra were collected at 0.6°/s scan speed between 10° to 90° 2Θ angles. The spectral resolution was 0.02°. No background correction for the presented spectra was applied.

2.3. Cyclic voltammetry

For electrochemical characterization, the powder samples were deposited from isopropanol-based suspensions onto a polycrystalline gold substrate ($d = 0.9$ cm) by targeting a uniform loading of 150 μg electrocatalyst per cm^2 (with the term electrocatalyst used for the system of nanoparticles and carbon support together). After drying, a capping layer of thin (0.1 μm) Nafion film was formed. The working electrode was held in hanging meniscus position in a conventional three-electrode electrochemical cell containing the Ar-saturated 0.5 M H_2SO_4 electrolyte. A platinum wire was used as auxiliary electrode and a glass-platinum reversible hydrogen electrode (RHE) unit as reference electrode. The scan rate was 50 mV/s.

2.4. Rotating disk electrode experiments

Electrocatalytic activity of the samples towards oxygen reduction in 1 M HCl was studied by the thin-film rotating disk electrode method [25]. A polished glassy carbon (GC) disk of 5 mm in diameter (Pine Instruments Company, USA) served as substrate for the powders. They were deposited onto the GC surface according to a procedure described elsewhere [22,25]. Briefly, the electrocatalyst was first ultrasonically suspended in isopropanol and a total of 18 μL volume of such suspension was dispersed on the GC surface via a micro-syringe in three steps. The suspensions were prepared so as to result a uniform 50 μg/cm^2 electrocatalyst loading on GC. After drying, a thin capping layer was formed by applying 16 μL of a 200 times-diluted 5 wt.% Nafion solution. The experimental setup was based on a Compact Pine Rotator (Pine Instruments Company, USA), and an Autolab PGSTAT-30 potentiostat (Eco Chemie B.V., Netherlands). The experiments were carried out in a conventional three-electrode glass cell containing the oxygen-saturated 1 M hydrochloric acid solution. A platinum wire and an Ag/AgCl (3 M NaCl) electrode were used as counter and reference electrodes, respectively. All electrode potentials in the manuscript are converted and refer to the RHE scale (0.24 V versus Ag/AgCl (3 M NaCl)). At least five thin film electrodes were prepared from each samples and good data reproducibility of the electrochemical response was found. (Data presented and analyzed here correspond to the anodic oxygen reduction scans collected at a sweep rate of 20 mV/s).

2.5. HCl electrolysis cell testing

To assess the ''real-life'' oxygen reducing activity and short-term corrosion behaviour of the electrocatalysts, the powdered samples were also incorporated into gas diffusion electrode [24]. All supported catalysts were tested in a 6.5 cm^2 active area cell, where their overall cell performance as working oxygen depolarized cathodes for the electrolysis of aqueous HCl was studied. This cell allowed for simultaneous measurements of both single and half cell data with the aid of various reference electrodes incorporated on both of its compartments. The cell temperature was 55 °C, the total cell back pressure was 2 atm while the cathodic compartment of the cell was fed with pure O_2 gas. The anode compartment was completely flooded with the anolyte liqueur comprised of Cl_2-saturated HCl (synthetic electrolyte having a concentration of 184 g/L of HCl). After keeping the cell under these conditions for approximately 3 h in

order to allow proper conditioning of the entire assembly, the overall performance of all the electrodes was tested under steady-state conditions.

3. Results and discussion

3.1. Physical and physicochemical characteristics

Typical nanoscale morphological characteristics of the carbon supported chalcogens were examined by scanning electron microscopy (SEM). Fig. 1 shows the SEM micrographs for the 30 (A), 15 (B), and 10 (C) wt.% supported Rh_xS_y powders. As readily apparent on the images, the chalcogen clusters take on a roughly spherical shape on the carbon flakes, similarly to metal nanoparticles. A statistical analysis of the number density of such clusters on a unit projected surface area combined with the analysis of the diameter used as the typical dimension of particles is applied to estimate the ultimate Rh_xS_y surface area exposed. The typical cluster size decreases linearly with decreasing Rh_xS_y loading, while the particle size exhibit a narrower size-distribution for the less-loaded samples as presented in Fig. 1. The average particle diameter is calculated to be 4.5 ± 1.5, 5.6 ± 2.1 and 8.3 ± 3.7 nm for the 10, 15 and 30 wt.% samples, respectively (Table 1). At the same time, the average number of particles on a unit planar surface area is more than twice as high for the 15 and 10 wt.% than for the 30 wt.% samples. Very similar ultimate cluster surface area values (within 5%) can be calculated for the 30 wt.% and 15 wt.% samples while at the 10 wt.% loading it is *ca.* two times smaller. In other words, the dispersion of Rh_xS_y is *ca.* two times higher in both the 15 wt.% and 10 wt.% carbon-supported samples than in the 30 wt.% Rh_xS_y/C.

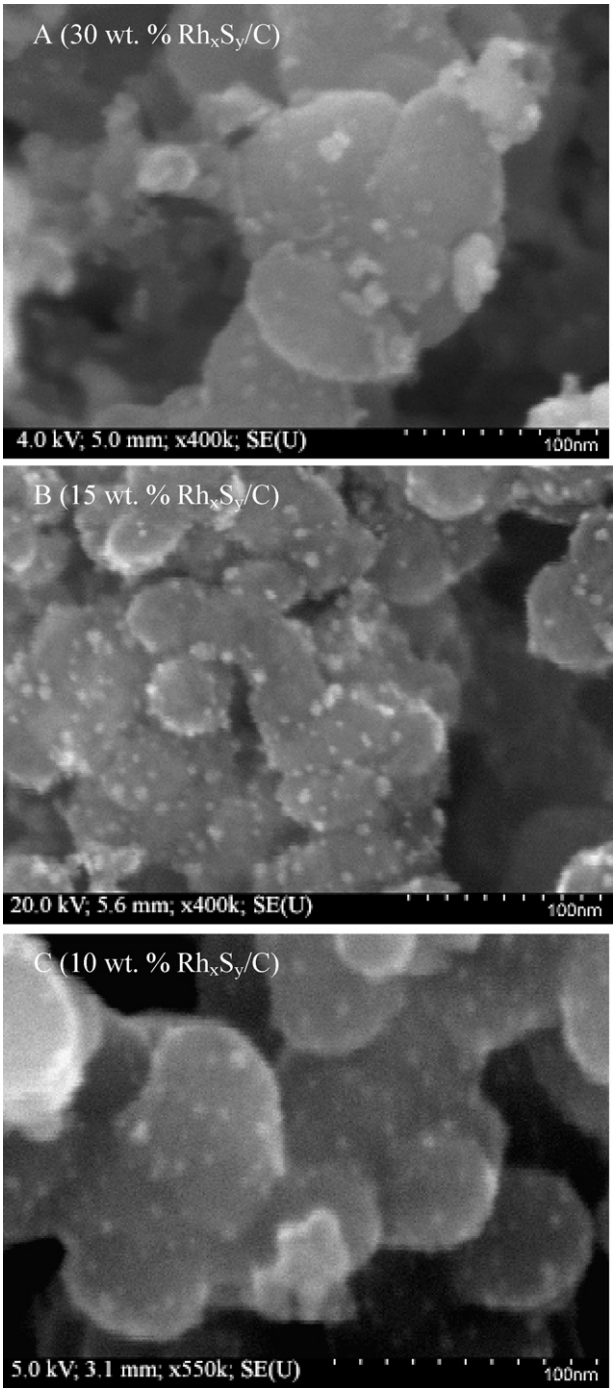

Fig. 1. Secondary electron SEM images taken for the (A) 30 wt.%, (B) 15 wt.%, and (C) 10 wt.% Rh_xS_y/C samples.

However, the benefit of having a higher dispersion does not necessarily translate to a higher mass-specific electrocatalytic performance. Such is the case for the carbon-supported platinum nanoparticle systems regarding the electroreduction of molecular oxygen. Platinum clusters size modifications induce changes in their surface morphology (faceting) and electronic properties ultimately impacting ORR activity, especially in the few nanometer dimension regime. This behaviour can particularly be expected from multi-element compounds such as the chalcogenides, which are known to have a rather complex and dynamically varying elemental composition and average (bulk) crystallographic characteristics depending on the preparation procedure. In the case of the crystal structure modifications of the rhodium/sulfur binary compounds, an extensive amount of research has been done in the past [22,26–32]. Although a detailed discussion of all the phases and crystallographic parameters present in the catalyst powders will be out of the scope of this manuscript, a summary of the state-of-the-art regarding the crystal structure of the sulfide compounds of the rhodium family is provided. Doing so will give the reader a broad view of the main phase structures observable in the X-ray patterns. In terms of crystal phase composition, the Rh_xS_y chalcogen family can be described by the following four different structures: (i) Rh_2S_3 [26,27], (ii) $Rh_{17}S_{15}$ [29], (iii) Rh_3S_8 [26] and, finally, (iv) the pseudo-spinel [22] Rh_3S_4. In our work, the Rh:S atomic ratios were assessed by energy dispersive X-ray spectroscopy and were found to be markedly larger (all values are above 1) for the supported samples as compared to unsupported (ca. 0.66 ± 0.10) one. Interestingly, the elemental composition in the 15 wt.% supported Rh_xS_y is found to be the most Rh rich (1.18 ± 0.04) compared to the 30 wt.% (1.05 ± 0.04) and 10 wt.% (1.10 ± 0.11) samples. It is also worth noting that the Rh:S atomic ratio for the 15 wt.% sample is found somewhat larger than for any of the single phase chalcogens (1.13 is the

Table 1
Physical and physicochemical characteristics for the *L* wt.% Rh_xS_y/C (*L* = 100, 30, 15, 10) and 30 wt.% Rh/C samples obtained by scanning electron microscopy imaging, electron dispersive spectroscopy and cyclic voltammetry

Sample	L (wt.%)	d (nm)	N[a] (particle μm^{-2})	γRh_xS_y[a]	Rh:S (at. ratio)	$E_{redn.}$[b] (V)
Rh/C	30	N/A	N/A	N/A	N/A	**0.43**
Rh_xS_y	N/A	N/A	N/A	N/A	**0.66** ± 0.10	N/A
Rh_xS_y/C	30	**8.3** ± 3.7	**2700** ± 500	**0.59** ± 0.02	**1.05** ± 0.04	**0.15**
Rh_xS_y/C	15	**5.6** ± 2.1	**6200** ± 500	**0.61** ± 0.01	**1.18** ± 0.04	**0.35**
Rh_xS_y/C	10	**4.5** ± 1.5	**5600** ± 500	**0.36** ± 0.01	**1.10** ± 0.11	**0.19**

[a] Corresponds to projected surface area.
[b] Peak potential of surface oxide reduction from the cyclic voltammogram (vs. RHE).

largest for the $Rh_{17}S_{15}$ phase) meaning that some of the Rh might not be incorporated into any of the major four single crystal structures.

Crystallographic changes upon varying Rh_xS_y loading on carbon have been observed by powder X-ray diffraction (XRD). Fig. 2 shows the XRD patterns for all of the chalcogen samples studied. The lineshapes are normalized to the intensity value of the main diffraction peak at *ca.* $2\Theta = 30^\circ$. From the analysis of the spectra, no evidence of the metallic Rh fcc lattice was found for any of the chalcogen samples; on the contrary, all of the spectral patterns seemed to exhibit the signatures of the single crystal chalcogenide phases. The XRD spectrum for the unsupported Rh_xS_y clusters clearly carries the features of the Rh_2S_3 structure [31,32], while lines corresponding to other crystal phases are difficult to assign. The observation of Rh_2S_3 phase as being the major constituent phase structure in the unsupported chalcogen was also attested by EDX analysis, from where exactly the 2:3 Rh:S atomic composition was determined. The spectral lineshape and structure for the supported Rh_xS_y samples are markedly different thus highlighting the role of carbon support in the development of chalcogen crystal structure. While a broad band emerging at *ca.* $2\Theta = 25^\circ$ corresponds to the carbon support, the chalcogen diffraction peaks collapse and become less resolved by

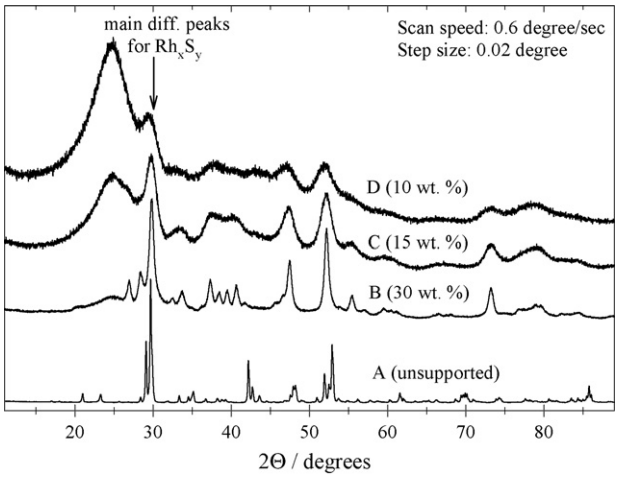

Fig. 2. Powder XRD patterns for the (A) unsupported (100 wt.%), (B) 30 wt.%, (C) 15 wt.% and (D) 30 wt.% Rh_xS_y/C samples. The spectra are normalized to the intensity of the main diffraction peak of the balanced-phase Rh_xS_y at *ca.* $2\Theta = 30^\circ$ indicated by an arrow.

lowering the Rh_xS_y loading on carbon (domain effect). They are believed to be superimposed on the broad bands of amorphous and/or transitional phases omitting a long range crystal order. The increasing intensity ratio of the carbon and main Rh_xS_y diffraction peaks by decreasing loading demonstrates how the long range-ordered crystallographic structure diminishes when the size of supported chalcogen clusters decreases below 10 nm. All supported chalcogen samples presented diffraction peaks corresponding to a balanced mixture of the $Rh_{17}S_{15}$ and Rh_3S_4 crystal structures as also reported by Beck and Hilbert [26]; although a small band, at $2\Theta = 21^\circ$ in the spectrum of the 30 wt.% sample, was observed which might be indicative of the presence of some Rh_2S_3 phase. Nevertheless, the diffraction bands between $2\Theta = 31^\circ$ and 42° and between $2\Theta = 42^\circ$ and 45° clearly mark the fingerprint of the $Rh_{17}S_{15}$ crystal phase and the Rh_3S_4 phases, respectively. Because of baseline drift issues, which are mainly the result of the increased contribution from amorphous/transitional phases, their relative distribution can only be judged at high 2Θ angles where contributions from only the long-range crystal structures are predicted. According to this presumption, the peak at *ca.* $2\Theta = 73.5^\circ$ corresponds to the $Rh_{17}S_{15}$ structure, while those at between ca. $2\Theta = 76^\circ$ and 81° is assigned to the Rh_3S_4 phase [26,31,32]. It is apparent that the relative ratio of $Rh_{17}S_{15}$ and Rh_3S_4 phases decreases by decreasing Rh_xS_y loading on carbon. However from the Rh:S ratio determined by EDX, it is possible to assume that the predominant phase remains $Rh_{17}S_{15}$ based on the fact that the overall ratio is greater than 1 even for the low loading samples. The argument that some of the excess Rh metal could be incorporated into amorphous/transitional phases, whose elemental composition is unknown, still remains valid. In addition, similar to Pt-based transition-metal alloy nanoparticles, segregation of elements in the clusters cannot be ruled out, which lead to noble metal-enriched small domains. Nevertheless, none of these enriched phases are evident based on long range diffracting domains.

The surface properties of these chalcogen samples have also been addressed by cyclic voltammetry in sulfuric acid electrolyte (Fig. 3). The cyclic voltammetric curve for the unsupported Rh_xS_y sample (medium dashed line) exhibits no significant capacitive or Faraday currents. Such behaviour can be readily understood by considering the predominant phase to be Rh_2S_3 structure composition, which appears to be completely inactive towards any redox behaviour in the

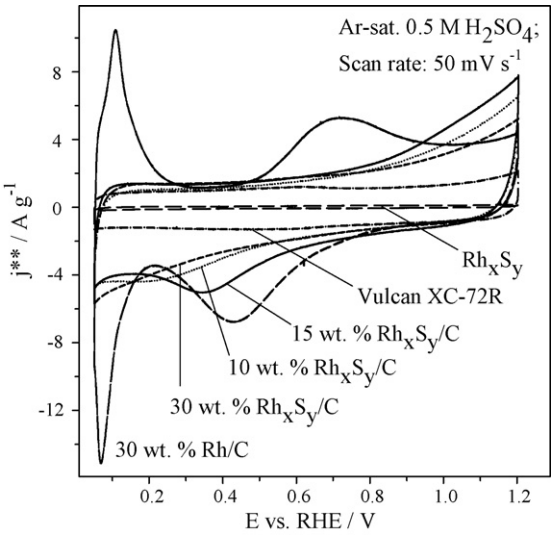

Fig. 3. Cyclic voltammetric curves for the 30 wt.% Rh/C (long-dashed line), unsupported (100 wt.%) Rh_xS_y (medium-dashed), 30 wt.% Rh_xS_y/C (short-dashed), 15 wt.% Rh_xS_y/C (solid), 10 wt.% Rh_xS_y/C (dotted) and Vulcan XC-72R (dash-dot) samples in Ar-saturated 1 M H_2SO_4 solution. The mass-specific current density values (j^{**}) were calculated after dispersing the electrocatalysts at a uniform 150 μg/cm^2 loading on the gold substrate (d = 0.9 cm).

operating potential window (0.0 to 1.2 V versus RHE). This can be understood on the basis of the inherent structure of Rh_2S_3, which has an orthorhombic *pbcn* structure with interspersed RhS_6 octahedra and SRh_4 tetrahedra providing for a bulk average Rh–Rh distance of 3.208 Å (compared to fcc Rh distance of 2.69 Å in pure Rh metal) and corresponding S–Rh_{avg} of 2.365 Å. Thus, the resulting structure is a bulk insulator, the only conducting domains are Rh rich layers (separated from each other by distances < 3.2 Å). As a result the electrochemical behaviour observed in Fig. 3 is most likely a combination of redox-inactive amorphous Rh rich domains and from presence of defects allowing the exposure of enough Rh planes within the Rh_2S_3 structure. By assessing the capacitive charging on the underlying Vulcan XC-72R carbon support (blank sample; dash-dot line), it is immediately clear that all of the carbon-supported Rh_xS_y systems show activity towards the electrosorption of certain aqueous species. However, when the comparison is made to the carbon-supported rhodium nanoparticles (long dashed line), it is also evident that there are significant differences in the proton adsorption/desorption region of the carbon-supported chalcogens. The lack of proton adsorption is a clear proof of the absence of purely metallic Rh (surface) domains in all the supported Rh_xS_y samples. This is also confirmed by the significant decrease of the measured Faraday currents compared to a 30 wt.% supported metallic Rh powder catalyst under electrode potential excursion. As also presented on the voltammograms (Fig. 3), surface oxidation and oxide reduction phenomena occur for the carbon-supported chalcogens as well, albeit with significant difference to supported Rh surface. Although the onset potential of OH^- adsorption on the supported Rh_xS_y samples seems quite close to that on the 30 wt.% supported metallic Rh system, significant oxide coverage develops at much larger overpotential in case of the chalcogen electrocatalysts. A thermodynamically preferred potential for the onset of oxide formation on the chalcogen is apparent only during the cathodic scan direction, thereby showing a common potential. More importantly, the 15% loading sample shows the highest oxidative mass specific currents (Fig. 3). In the given experimental conditions, the peak potential of the oxide reduction wave is observed at 0.42 V, 0.15 V, 0.34 V and 0.17 V for the 30 wt.% supported Rh metal, 30 wt.% Rh_xS_y, 15 wt.% Rh_xS_y and 10 wt.% Rh_xS_y supported chalcogens, with the most positive value recorded for the 15 wt.% supported Rh_xS_y clusters approaching to that of measured for supported 30 wt.% Rh nanoparticles. Table 1 shows the magnitude of electrochemical charge associated with surface oxidation/reduction processes which is almost twice as much for the 15 wt.% sample as compared to the 30 wt.% supported chalcogen sample. Among all investigated electrocatalysts including the supported rhodium nanoparticle system, the highest rhodium mass-specific surface oxide formation/reduction charge was calculated for the 15 wt.% supported Rh_xS_y sample. The higher capability of the low loading (<30 wt.%) chalcogen samples to adsorb oxides and also to reduce them at a lower overpotential suggests a possible higher noble metal utilization for the electroreduction of molecular oxygen as well.

3.2. Oxygen reduction activity

The kinetics of the reduction of molecular oxygen on the chalcogen surfaces was studied by using the thin-film rotating disk electrode method, and was benchmarked to data obtained for platinum and rhodium electrocatalyst systems in the same conditions. In relevance to hydrochloric acid electrolysis cell applications, where the presence of chloride ions at the oxygen depolarized cathode can be expected, the experiments were carried out in oxygen-saturated 1 M HCl. In this media, especially under voltage cycling in the usual electrode potential region (*i.e.* between the thermodynamic equilibrium potential of oxygen reduction and the onset potential of hydrogen evolution), dissolution of transition metals is expected to occur. In fact, both the 30 wt.% supported metallic Rh and the 30 wt.% supported metallic Pt samples exhibited notable instability under voltage cycling resulting in gradually collapsing proton under potential deposition (UPD) regions as well as RDE polarization curves (data not presented here). The UPD region refers to the electrodeposition of metal monolayer(s) on a foreign metal substrate at potentials that can be significantly less negative than that for the deposition on the same metal surface as the adsorbate [33]. On the other hand, no changes in the electrochemical responses were observed for all of the supported Rh_xS_y samples. Although the Levich criterion was met only with the chalcogen systems (*i.e.* linear relationship stands between the limiting current and the square root of the rotation rate), for the sake of data comparison and interpretation we decided to use the first cycle only for pure transition metal systems in order to assess the inherent ORR activity of electrocatalysts when the noble metal content is known.

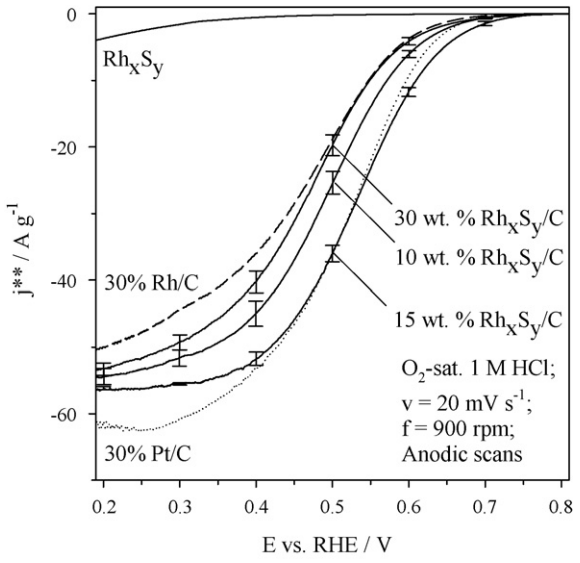

Fig. 4. ORR polarization curves obtained by using an RDE setup in O_2-saturated 1 M HCl for the 30 wt.% Rh_xS_y/C, 15 wt.% Rh_xS_y/C and 10 wt.% Rh_xS_y/C (solid lines), 30 wt.% Pt/C (dotted) and 30 wt.% Rh/C (dashed) electrocatalysts. The mass-specific current density values (j**) were calculated after dispersing the electrocatalysts at a uniform 50 μg/cm^2 loading on the glassy substrate (d = 0.5 cm).

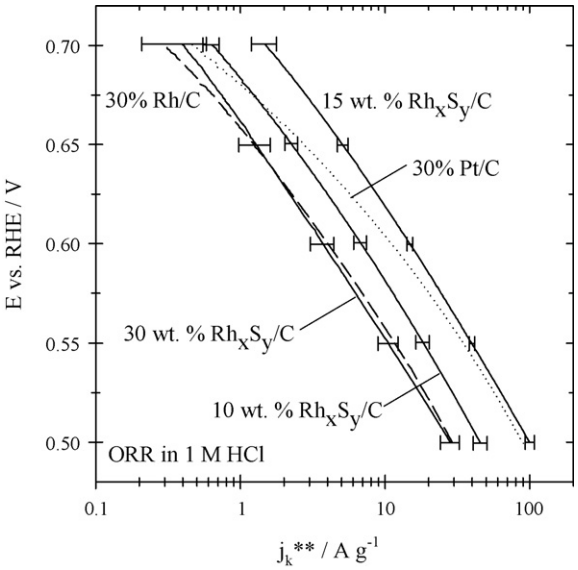

Fig. 5. Mass-transport corrected Tafel-plots for ORR in 1 M HCl for the 30 wt.% Rh_xS_y/C, 15 wt.% Rh_xS_y/C and 10 wt.% Rh_xS_y/C (solid lines), 30 wt.% Pt/C (dotted) and 30 wt.% Rh/C (dashed) electrocatalysts. Data were obtained by using RDE (Fig. 4).

Fig. 4 shows the representative ORR polarization scans taken in identical conditions for the carbon supported chalcogen and pure metal clusters. Thin film RDE electrodes made of the powdered samples were reproduced at least five times in order to ensure conclusive data for comparison. The sufficiently small standard deviations of the calculated electrocatalyst mass-specific current density values are demonstrated for the supported Rh_xS_y samples. By looking at the reduction waves, it is immediately evident that the unsupported Rh_xS_y exhibits no significant activity towards the electroreduction of molecular oxygen. All of the supported Rh_xS_y samples however, outperform the 30 wt.% supported metallic Rh and show comparable activity to that of the commercial 30 wt.% supported metallic Pt. The mass transport-corrected mass-specific kinetic current density (j_k**) values for oxygen reduction are summarized in Table 2. We must emphasize that j_k** refers to the total electrocatalyst mass (*i.e.* to the summed mass of the nanoparticles and of the carbon support). The most striking conclusion is that the low-loading (15 and 10 wt.%) supported Rh_xS_y electrocatalysts enable much higher activity at the lower ORR overpotential region (at 0.7 V) than the standard (30 wt.%) supported Rh_xS_y and the supported Rh metal electrocatalyst. In particular, the current-density for the 15 wt.% chalcogen is *ca.* five-, four- and three-times larger than those for the 30 wt.% supported Rh metal, 30 wt.% supported Rh_xS_y and 30 wt.% supported Pt metal, respectively. By considering that only *ca.* the three-quarters of the total Rh_xS_y weight is of Rh metal for the supported chalcogen clusters, these data translate to a *ca.* 13- and 11-times higher utilization of the precious Rh metal in ORR in the 15 wt.% supported Rh_xS_y compared to those in the 30 wt.% supported Rh metal, 30 wt.% supported Rh_xS_y, respectively. While the kinetic advantages by the low-loading supported rhodium sulfides is preserved in the entire electrode potential region over the standard supported chalcogen system, the metal-based electrocatalysts become comparable with the supported chalcogens at high ORR overpotential (at and above 0.5 V). In fact, the half wave potential values (from Fig. 4) were found at 0.50 ± 0.1 V for all electrocatalysts, which are considerably lower values than those observed for the transition metal nanoparticle systems (for supported Pt and Rh metals) in non-adsorbing electrolytes (in TFMSA, or $HClO_4$). Therefore the

Table 2
Oxygen reduction activity parameters for the L wt.% Rh_xS_y/C (L = 30, 15, 10), 30 wt.% Pt/C and 30 wt.% Rh/C electrocatalysts as determined from rotating disk electrode experiments and single HCl electrolysis cell testing

Sample	j_k**[a] (A g^{-1})		b (mV decay^{-1})		E_{cell}[a]. (V)	
	0.70 V	0.50 V	0.70–0.65 V	0.55–0.50 V	1 kA m^{-2}	5 kA m^{-2}
30 wt.% Pt/C	**0.46**	**88.59**	**65**	**122**	N/A	N/A
30 wt.% Rh/C	**0.28**	**29.13**	**82**	**127**	N/A	N/A
30 wt.% Rh_xS_y/C	**0.39**	**28.36**	**100**	**117**	**0.800**	**1.280**
15 wt.% Rh_xS_y/C	**1.48**	**100.41**	**95**	**125**	**0.778**	**1.318**
10 wt.% Rh_xS_y/C	**0.63**	**45.00**	**90**	**126**	**0.845**	**1.340**

[a] Standard deviation of data are plotted on the corresponding figures.

shift in the onset potential is attributed to the strong adsorption of chloride ions, which block those surface sites that are active for ORR. As a consequence, the ORR polarization lines for the pure metals (especially for platinum) rise steeper between the mass transport and kinetically controlled potential region in HCl. This observation is also confirmed by the fact that the reduction waves for the chalcogen electrocatalysts follow the same sinusoidal shape thus suggesting a similarly moderate influence of chloride ion adsorption, if any, on ORR.

Fig. 5 compares the trends in ORR kinetics in 1 M HCl electrolyte by comparing the mass transport-corrected Tafel plots for the investigated electrocatalysts. Interestingly, only the 30 wt.% supported Pt/C electrocatalyst exhibits two Tafel slopes, one −65 mV/decay at between 0.70 V and 0.65 V, and other −122 mV/decay at between 0.55 V and 0.50 V (Table 2). On the other hand, the Tafel plots for the supported rhodium and rhodium chalcogen samples are monotonely curving and in the low ORR overpotential region the fitted slopes are somewhat higher (above 80) than that determined for platinum. Since the number of electrons involved in ORR has not yet been analyzed for the chalcogen samples in HCl, (by measuring hydrogen peroxide yield on a ring electrode), any conclusions on the reaction mechanism are still to come.

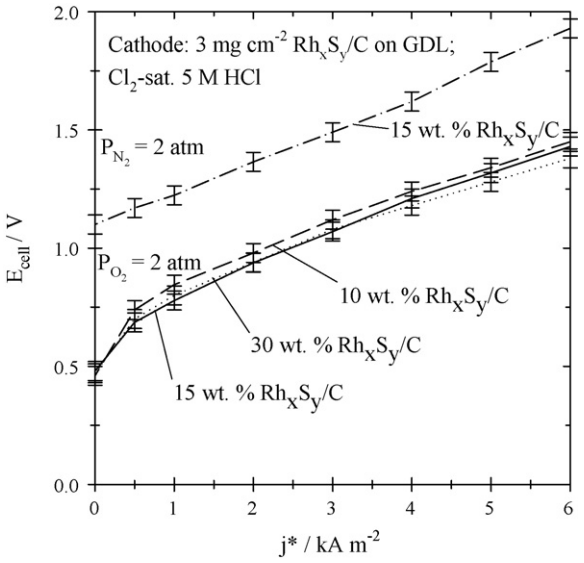

Fig. 6. Single cell polarization data under the electrolysis of Cl_2-saturated 1 M HCl electrolysis for the 30 wt.% Rh_xS_y/C (dotted line), 15 wt.% Rh_xS_y/C (solid) and 10 wt.% Rh_xS_y/C (dashed) ODC electrocatalysts dispersed at a uniform 3 mg cm^{-2} loading on the GDL. Data for the 15 wt.% Rh_xS_y/C sample (point-dash) is also shown when used as hydrogen evolving cathode. The current density values refer to the geometric surface area (6.5 cm^2).

3.3. ODC performance in a single cell HCl electrolyzer

To further support and validate the advantage of this novel class of electrocatalysts, all supported chalcogen samples were transformed into GDEs and tested into a ''real-life'' scaled-down electrolyzer cell as ODC. Just as in case of the RDE experiments, the electrocatalysts were applied in a uniform but higher 3 mg/cm^2 loading on a commercial carbon cloth gas diffusion electrode, *i.e.* the 15 wt.% supported Rh_xS_y ODC contained *ca.* twice, while the 10 wt.% supported Rh_xS_y ODC *ca.* three-times less precious metal (Rh) compared to the standard 30 wt.% supported Rh_xS_y standard ODC. Fig. 6 shows the steady state polarization curves for all samples. In the particular case of the 15 wt.% supported Rh_xS_y electrode, the H_2 evolution curve is also shown (dot-dash line) in order to further demonstrate the magnitude of the improvement relative to the standard 30 wt.% supported Rh_xS_y electrocatalyst. Considering a standard deviation of *ca.* 0.04 V for the data, roughly 0.5 V savings could be attained with all the three chalcogen samples when used as ODC electrocatalysts. Table 2 summarizes the cell potential values, in the low current density region where ORR kinetics is expected to limit the overall cell performance (at and below 1 kA/m^2). As seen, the 15 wt.% supported Rh_xS_y electrode outperforms the standard 30 wt.% supported chalcogen sample. The advantage of a more facile and efficient ORR kinetics however, vanishes at higher current demands and it becomes also less obvious for the 10 wt.% chalcogen sample (Fig. 6 and Table 2). Such penalization is not related to the inherent electrocatalytic activity of the chalcogen clusters but likely the result of a hindered mass-transport of reactants and products in the gas diffusion layer of the ODC electrode. While the scope of this work was to provide a better understanding of the electrocatalyst as such, no attempt was made to optimize the electrode architecture and structure. Simply put, the low loading GDE contains twice as much carbon compared to the standard 30 wt.% GDE; thus suggesting a fundamentally different mechanism of how water is being transported in the gas diffusion electrode. Changes in the electrode's architecture and hydrophobic characteristics are therefore expected to influence oxygen transport and water management in the ODC. Nevertheless, mass transport phenomena can be improved by optimizing the structure of the gas diffusion electrode and the benefits of better electrocatalysis can also be fully capitalized on the entire range of cell operation. Further studies targeting this issue are currently underway and their results will be the objective of our future work. It is noteworthy that during the small electrolyzer tests, no detectable decay in performance and or degradation of GDE was detected. Moreover, preliminary corrosion testing data suggest that the carbon-supported low-loading chalcogen electrocatalysts are even less prone to noble metal dissolution than the standard 30 wt.% supported sample. Our findings are of high practical significance since they put the low-loaded electrocatalyst (15 wt.% supported Rh_xS_y) not only much more cost efficient position but with those samples the overall cell performance on the standard GDE (30 wt.% Rh_xS_y) in a ''real-life'' application can be matched thus extending the viability of the hydrochloric acid electrolysis on an industrial scale.

4. Conclusions

A novel class of rhodium sulfide chalcogens featuring various Rh_xS_y loading on Vulcan XC-72R carbon was studied in the context of oxygen depolarized cathode electrocatalysis for the hydrochloric acid electrolysis process. Electron microscopy imaging revealed that the dispersion of the chalcogen clusters

on the carbon support could be optimized by reducing the loading of the commercially available 30 wt.% catalyst down to 15 wt.% while maintaining the same support (Vulcan XC72-R, Cabot Corp.). In addition to the more desired physical-chemical characteristics obtainable with the low-loading samples, particularly in terms of surface oxide formation/reduction, higher catalyst utilization and catalyst efficiency is also observed. The results revealed the intimate relation existing between the Rh_xS_y moieties and its loading level on the selected support, as also revealed by EDS and powder XRD data presented. In terms of ''real-life'' applications, it was found that it is possible to efficiently and effectively reduce the precious metal loading by as much as three times in the ODC without any detrimental penalization in terms of cell performance as well as catalyst durability. Overall, these findings constitute a major advancement in the commercialization and implementation of the novel oxygen-consuming gas diffusion electrode (GDE) technology.

Acknowledgements

This work has been accomplished, thanks to the financial and intellectual support the *E-TEK* division of PEMEAS Fuel Cell Technologies, Inc. (NJ) and it is registered with the Office of Patents and Trademarks under the following numbers; US 6,967,185, US 6,149,782 and U.S. 6,358,381. The authors wish to gratefully thank Dr. Hakim Nazih for his collaboration during the collection of the SEM micrograph data.

References

[1] F. Federico, G.N. Martelli, D. Pinter, Gas-Diffusion Electrodes for Chlorine-Related (Production) Technologies, vol. 8, Modern Chlor-Alkali Technology, 2001, pp. 114–127.
[2] R.J. Allen, et al., Rhodium Electrocatalyst and Method of Preparation, De Nora S.p.A (IT), USA, 2000.
[3] R.J. Allen, A.F. Gullá, Synthesis of Noble Metal Sulphide Catalyst in a Sulfide Ion-Free Aqueous Environment, De Nora Elettrodi S.p.A. (IT), US, 2005.
[4] A.F. Gullá, R.J. Allen, E.S. De Castro, Catalyst for Oxygen Reduction, De Nora S.p.A. (IT), USA, 2004.
[5] E.N. Balko, SPE hydrochloric acid electrolysis cell: performance Cell Configuration, in: Oronzio DeNora Symposium-Chlorine Technology, 1979.
[6] E.N. Balko, Anode for reducing Oxygen Generation in the Electrolysis of Hydrogen Chloride, General Electric Co., Wilmington, MA, USA, 1980
[7] E.N. Balko, High Temperature and Low Feed Acid Concentration Operation of HCl Electrolyzer Having Unitary Membrane Electrode Structure, General Electric Company, Wilmington MA, USA, 1981.
[8] F.R. Minz, HCl-electrolysis-technology for recycling chlorine, in: Conference on Electrochemical Processing,Innovation and Progress, Glasgow, UK, 1993.
[9] T.J. Schmidt, et al. J. Electroanal. Chem. 508 (1–2) (2001) 41–47.
[10] Gestermann, F., et al., Electrode for conducting electrolysis in acid media, in: PCT Int. Appl., Bayer Aktiengesellschaft, Germany and De Nora Elettrodi SPA: Germany, 2003. p. 17.
[11] G. Horanyi, M. Wasberg, J. Electroanal. Chem. 404 (2) (1996) 291–298.
[12] R. Cote, et al. J. Mater. Electrochem. Syst. 1 (1) (1998) 7–16.
[13] N. Alonso-Vante, H. Tributsch, Nature (London, United Kingdom) 323 (6087) (1986) 431–432.
[14] N. Alonso-Vante, H. Tributsch, J. Electroanal. Chem. Interfacial Electrochem. 229 (1-2) (1987) 223–237.
[15] N. Liu, et al. J. Catal. 215 (2) (2003) 254–263.
[16] N. Alonso-Vante, et al. J. Am. Chem. Soc. 109 (11) (1987) 3251–3257.
[17] N. Alonso-Vante, B. Schubert, H. Tributsch, Mater. Chem. Phys. 22 (3–4) (1989) 281–307.
[18] G.J. Miller, J. Alloys Compd. 229 (1) (1995) 93–106.
[19] K.A. Gschneidner Jr., J. Mater. Eng. Perform. 7 (5) (1998) 656–660.
[20] M. Rabiller-Baudry, R. Chevrel, M. Sergent, J. Alloys Compd. 178 (1992) 441–445.
[21] O. Solorza-Feria, et al. Electrochim. Acta 39 (11–12) (1994) 1647–1653.
[22] O. Solorza-Feria, et al. Thin Solid Films 311 (1–2) (1997) 164–170.
[23] H. Tributsch, et al. J. Appl. Electrochem. 31 (7) (2001) 739–748.
[24] R.Lindstrom, R.J. Allen, J. Walter, Thin carbon-cloth-based electrocatalytic gas diffusion electrodes and electrochemical cells comprising them, in European Patent Office, Prototech Co., USA, 1981, p. 31.
[25] U.A. Paulus, et al. J.Electroanal. Chem. 405 (2001) 134–145.
[26] J. Beck, T. Hilbert, Z. Anorg. Allg. Chem. 626 (2000) 72–79.
[27] S. Geller, Acta Crystallogr. 15 (1962) 1198–1201.
[28] M. Ishii, et al. Solid State Ionics 136-137 (2000) 403–407.
[29] E. Parthe, D. Hohnke, Acta Crystallogr. 23 (1967) 832–840.
[30] B. Schubert, et al. Electrochim. Acta 41 (9) (1996) 1471–1478.
[31] J.M. Ziegelbauer, et al. Electrochem. Solid-State Lett. 9 (9) (2006) A430–A434.
[32] J.M. Ziegelbauer, et al., In situ X-ray absorption spectroscopy characterizations of Rh_xS_y for ORR applications, in: 232nd ECS National Meeting, American Chemical Society, San Francisco, CA, United States, 2006.
[33] E. Herreo, L.J. Buller, H.D. Abruna, Chem. Rev. 101 (2001) 1897–1930.